Lab on a Chip

PAPER

View Article Online
View Journal | View Issue

Cite this: *Lab Chip*, 2021, **21**, 3128

Microfluidic chip grafted with integrin tension sensors for evaluating the effects of flowing shear stress and ROCK inhibitor on platelets†

Subin Mao,‡[a] Anwesha Sarkar,‡[ab] Yongliang Wang,[b] Chao Song,[a] Dana LeVine,[c] Xuefeng Wang*[b] and Long Que*[a]

Integrins are key players in platelet adhesion and aggregation. Integrin molecular tensions, the forces transmitted by integrin molecules, are regulated by both mechanical and biochemical cues, and the outside-in and inside-out signaling has been extensively studied. While the mechanical properties of platelets at static status have been studied by atomic force microscopy, traction force microscopy and tension sensors, the biomechanical properties of flowing platelets remain elusive. Herein, we report microfluidic chips grafted with integrin tension sensors for microfluidic-force mapping in platelets. Specifically, the process of integrin $\alpha_{IIb}\beta_3$ mediating tension transmission and platelet adhesion under low flow rates has been obtained, and the process of platelet clustering at post-stenotic regions has been demonstrated. We found that flowing shear force can postpone the integrin-mediated tension transmission and platelet adhesion. We further evaluated the effect of Y-27632, a ROCK inhibitor that has been proven to reduce integrin-mediated platelet adhesion, at a series of concentrations and demonstrated that microfluidic chips with integrin tension sensors are sensitive to the concentration-dependent effects of Y-27632. Given their low cost and scalable throughput, these chips are ideal technical platforms for biological studies of platelets at flowing status and for platelet inhibitor or potential antiplatelet drug screening.

Received 27th March 2021,
Accepted 17th June 2021

DOI: 10.1039/d1lc00259g

rsc.li/loc

Introduction

Cardiovascular diseases are the major cause of death globally.[1] In 2015, 17.7 million people died from cardiovascular diseases, representing 31% of all global deaths (facts listed by the World Health Organization). Thrombosis is the most common pathology causing life-threatening cardiovascular diseases such as ischemic heart disease, stroke, and venous thromboembolism. Primary hemostasis, a process of stopping bleeding from small vessels, is mediated by platelets.[2–4] However, during thrombosis, platelets can abnormally adhere to blood vessel walls and promote cell-based coagulation and subsequent fibrin generation, resulting in blood clots that cause heart attacks, strokes, and peripheral vascular disease.[5] Such abnormal platelet adhesion can be initiated by ruptured cholesterol plaques in blood vessels or by disturbed blood flow in areas of vascular stenosis, or narrowing. As mentioned in ref. 6, variation of hemodynamic parameters involved in blood flow influences thrombus formation and shear rates vary from zero to 1500 s^{-1} among different parts of the arterial tree. A clear correlation between platelet deposition and shear rate has been described. At zero shear rate, platelet deposition was $(5.2 \pm 2.8) \times 10^6$ platelets per cm^2 and a maximum shear rate of 1500 s^{-1} yielded platelet deposition of $(64.7 \pm 8.3) \times 10^6$ platelets per cm^2. Fibrin deposition was elevated similarly with increasing shear rate, demonstrating the importance of shear rate in platelet and fibrin deposition and thrombus formation. Because the local blood flow and shear conditions are important mechanical factors initiating platelet adhesion and activation, studying platelet functions under controllable flow conditions is desired for the understanding of the mechanism of thrombus formation. Previously, Chen *et al.*[7] discussed mechanisms through which cell-generated forces, external forces applied on the cell and variation of substrate mechanics could bring about changes in cell function through mechanotransduction pathways. Using atomic force microscopy, Lam *et al.*[8] observed the contraction dynamics, measured the mechanics of single platelets and discovered the maximum contractile force that platelets can generate.

[a] *Electrical and Computer Engineering Department, Iowa State University, Ames, USA50011. E-mail: lque@iastate.edu*
[b] *Department of Physics and Astronomy, Iowa State University, Ames, USA50011. E-mail: xuefeng@iastate.edu*
[c] *Veterinary Clinical Sciences, Iowa State University, Ames, USA50011*

† Electronic supplementary information (ESI) available: Two figures in the supplementary document. See DOI: 10.1039/d1lc00259g

‡ These authors contributed equally.

When they encountered environments with higher rigidity, platelets yielded larger stall forces, demonstrating the possibility of heterogeneous contraction of blood clots by platelets. Myers *et al.*[9] quantified single-platelet contraction forces in varying clot environments and revealed that platelets combine biochemical and mechanical inputs to go through contraction. Through multiscale simulations, King *et al.*[10] showed the process of adhesion of platelets and growth of thrombus.

Initial adhesion and activation of platelets in blood flow are orchestrated by both biochemical and mechanical factors. The external mechanical force most relevant to platelet adhesion and activation in blood vessels is the shear stress of blood flow on the vessel wall.[11] Shear stress is the product of blood shear viscosity η (2.8 mPa s) and shear rate. The pull/shear force on individual adherent platelets caused by the local shear stress can be estimated using the equation $F = \eta A\dot{\gamma}$, where $\dot{\gamma}$ is the shear rate and A is the area of adherent platelets ($\sim 10^{-10}$ m^2). As platelets must counteract this pull/shear force during thrombus formation, the shear stress likely plays critical roles in platelet tethering and adhesion in hemostasis by influencing the platelet adhesion force and contraction force. Multiple receptors mediate platelet adhesion and contraction on blood vessel walls. At a high flow rate ($>10\,000$ s^{-1}), glycoprotein Ib-V-IX (GPIb-IX-V) tethering to von Willebrand factor (vWF) initiates the platelet adhesion without the participation of integrins $\alpha_{IIb}\beta_3$.[12] After the initial tethering, integrin $\alpha_5\beta_1$ (glycoprotein Ic–IIa) and integrin $\alpha_{IIb}\beta_3$ (glycoprotein IIb–IIIa)[13–15] regulate the stable platelet adhesion, spreading, aggregation and contraction.[16–18] At a flow rate of <1000 s^{-1}, active integrins $\alpha_{IIb}\beta3$ are capable of binding to the subendothelial ligands directly.[19] Being indispensable in hemostasis and thrombosis, integrin $\alpha_{IIb}\beta_3$ is known to transmit cellular force which is essential for the retraction and stabilization of the blood clot. Therefore, visualizing and mapping platelet force transmitted by the GPIb-V-IX receptor and integrin $\alpha_{IIb}\beta_3$ under shear stress will likely reveal valuable biomechanical information about the mechanism of platelet adhesion and contraction that leads to thrombus formation in blood vessels.

The biomechanical regulation in platelet function has been performed by a variety of techniques such as atomic force microscopy (AFM),[20,21] traction force microscopy,[22,23] and integrin tension sensors.[24] Among integrin tension sensors, DNA engineering has been previously used in tension gauge tether (TGT) design,[25–27] and the hairpin DNA structure was modified in monitoring receptor–ligand tension in real time.[28,29] Since the sensor size is only a few nanometers, it allows us to detect a single macromolecular tension, like integrins. In principle, the double-stranded DNA fragment was immobilized on a glass surface by the bottom strand and the RGD peptide (integrin ligand) was conjugated onto the upper strand (Fig. 1A), as the RGD motif in vWF and fibrinogen is recognized by integrin $\alpha_{IIb}\beta_3$.[30,31] The pairing or bonding between nucleotides will be overcome when the integrin tension is high enough. Using this tool, the platelet biomechanics with high data throughput at submicron resolution has been investigated.[24]

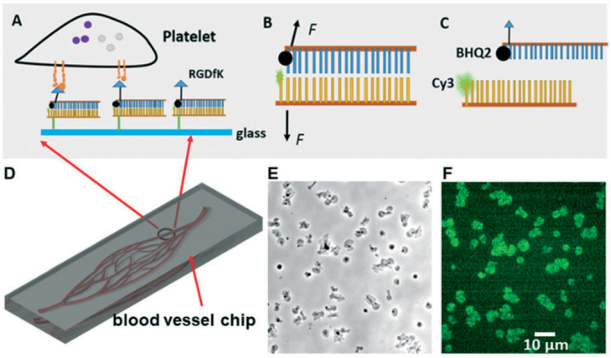

Fig. 1 (A–C) Schematics showing the integrin tension sensor structure and its operating principle. (D) Schematic of a blood vessel-mimicking chip: the platelets are flowed through microfluidic channels coated with integrin tension sensors. The tension of integrin $\alpha_{IIb}\beta_3$ is reported by the fluorescence signal if the tension overcomes the bond between the two strands of the dsDNA. (E) Representative optical micrograph of integrin tension sensors and platelets. (F) The corresponding force mapping (fluorescence image) in the blood vessel-mimicking microfluidic channel.

As mentioned in our previous work,[24] platelet force map resolution on an integrative tension sensor platform has been calibrated. The integrin tension sensor (ITS) reports force distribution directly through fluorescence imaging (Fig. 1A–C). The Cy3 fluorophore in ITS is quenched by the BHQ2 quencher (95% quenching efficiency) when no force is applied for mechanical separation of dsDNA, yielding almost zero fluorescence (Fig. 1B). Once platelet receptor integrins form bonds with RGD in the ITS, tension transmission to the ITS occurs during platelet adhesion and contraction. The transmitted tension is capable of separating dsDNA and making Cy3 unquenched by freeing Cy3 from the quencher (Fig. 1C). The ITS retains fluorescence once it is activated. As a result, all integrin tensions larger than the ITS tension threshold will be reported. Signal integration of this kind keeps the force footprint intact even after the cells are immunostained or removed, enhances the sensitivity greatly, and yields high fluorescence intensity. The ITS copy number per unit area was determined to be 1200 μm^{-2}.[24]

In our previous study, we demonstrated the existence of two levels of integrin tensions in platelets at static status.[24] Here, we investigated how platelets behave in flowing status at the single molecular level since flowing status is more relevant to the *in vivo* conditions. In this work, we designed a series of microfluidic chips (straight-microchannel chip, single blood vessel mimicking chip composed of curved microchannels, and blood vessel-mimicking chips with an integrated solution concentration gradient generator) integrated with integrin tension sensors (Fig. 1A–D), in which the glass surface of the microfluidic channels was coated with ITS that will fluoresce when the integrin tension is higher than the threshold or tension tolerance

(Fig. 1B and C). As an example, representative optical images and the corresponding fluorescence images of the integrin tension sensors are shown in Fig. 1E and F. In this case, the pairing between nucleotides is separated by the integrin tension resulting from the adhesion of platelets, dismantling the quencher from the dye and enabling the tension sensor to emit fluorescence.

Specifically, we report our recent studies by using platelet force maps as cell mechanical fingerprints to assess platelet behaviors under (i) flowing shear stress including post-stenotic shear stresses and (ii) Y-27632 (ROCK inhibitor) treatment using microchips. By controlling the flow rate, various shear stresses were applied to platelets, and at a certain range of low flow rate (tested 1–100 s^{-1}), platelets adhered and retracted their integrin ligand RGD, and the recorded force pattern shows several force-enriched foci. In addition, since antiplatelet drugs can reduce the chance of myocardial infarction by reducing platelet aggregation and preventing pathologic thrombosis, the effect of Y-27632 (ROCK inhibitor that has been proven to reduce integrin-mediated platelet adhesion) on the biomechanical behaviors of platelets was also evaluated.

In this study, canine platelets were adopted for the mechanobiological study of platelets in a microfluidic chip due to the higher accessibility of dog blood than human blood. Dog platelets possess comparable biological traits to human platelets[32] and dogs are close to humans sizewise, yielding similar metabolic rates and rheology in blood.[33] Furthermore, signaling pathways, platelet sizes and platelet counts of dogs are similar to those of human platelets.[34]

There are also similarities between human and canine cardiovascular disease. Although dogs rarely suffer from myocardial infarction, other common human cardiac diseases like dilated cardiomyopathy and chronic valvular disease are very common in dogs.[35] Furthermore, human and canine hearts share many similar characteristics at the cellular and organ levels.[36] In addition to prothrombotic diseases, dogs also spontaneously develop immune thrombocytopenia, an autoimmune disease targeting platelets and leading to severely decreased platelet counts. Dogs provide an excellent model of this human disease, which can lead to fatal hemorrhage and thus provide a good platform to assess medications that might aid in platelet function and hemostasis.[32] As a result of all these similarities, canine platelets represent a good translational model for human platelet mechanobiology.

Materials and methods

A. Materials and imaging

Polydimethylsiloxane (PDMS) and its curing agent were purchased from Dow Corning, Inc. SU-8 photoresist was purchased from MicroChem, Inc. Deionized (DI) water was obtained from a DI water purification system (Millipore, France). Y-27632, Rho-associated kinase (ROCK) inhibitor, was purchased from Sigma-Aldrich, Inc. A fluorescence microscope (Nikon Ti-E2) was used to obtain the fluorescence images of the platelets.

B. Microfluidic chip design and fabrication

Design and simulation of the straight-microchannel chip for studying flowing rate/stress effect. The size of the channel was 80 μm (height) × 100 μm (width), while the stenosis mimic channel was designed with 50 μm width at the narrow region and 100 μm at the wide region (Fig. 2A). The velocity profile and the corresponding shear stress on the platelets inside the wide channel (CH_W) and the narrow channel (CH_n) were calculated using COMSOL. To facilitate the simulation, some platelets (Fig. 2B) were assumed to be distributed and mechanically fixed inside the regions of the wide channel and the narrow channel. In the model, the size of the platelets was assumed to be 3 μm in diameter.[33,37]

Chip for mimicking blood vessel and ROCK inhibitor treatment with a solution concentration gradient generator. Different from the straight-microchannel chip, a microfluidic chip with a more complicated microchannel network was designed and fabricated to reflect the complexity of the blood vessel network. In this effort, this chip was only used to evaluate the ROCK inhibitor effect on platelets.

For simplicity, the sizes of all curved channels in the blood vessel mimicking chip (Fig. 3A and B) were kept the same at 80 μm (height) × 100 μm (width). The solution concentration gradient generator (Fig. 3C) was adapted from the tree-shaped microfluidic chip.[38] The size of the channels was 80 μm (height) × 100 μm (width) with three inlets, 1, 2, and 3.

Chip fabrication process. A silicon wafer substrate was cleaned with acetone, IPA and DI water in sequence. SU8-2075 photoresist was then spin-coated onto the silicon wafer substrate spinning at 3000 rpm for 60 seconds to achieve a coating with an approximate thickness of 80 μm. An SU8 mold was then fabricated using standard optical lithography. Liquid PDMS polymer with curing agent was then poured onto the SU8 mold and cured at 65 °C for 2 hours. The PDMS layer was then peeled off from the SU8 mold, followed by making inlets and outlets using a biopsy punch. The PDMS

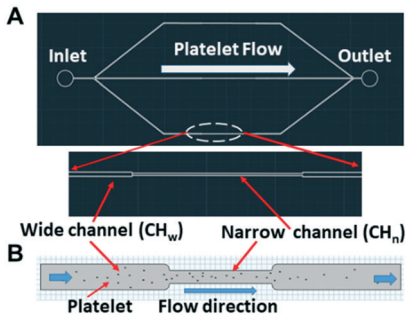

Fig. 2 (A) Sketch of a microfluidic chip for studying the platelets under flowing status in the stenotic region (narrow region) *vs.* the non-stenotic region. (B) Sketch showing the platelets inside the wide channel and narrow channel for simulations.

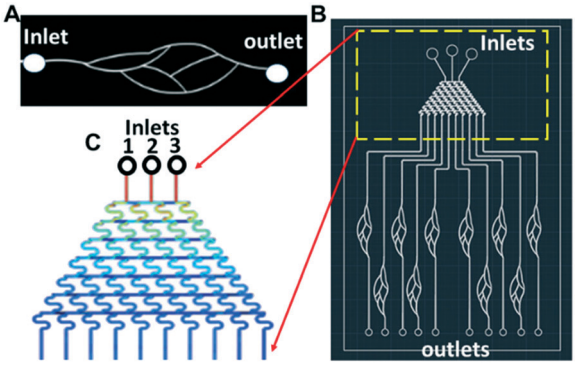

Fig. 3 (A) Sketch of a single blood vessel mimicking chip. (B) Sketch of a chip consisting of ten blood vessels integrated with a solution concentration gradient concentration generator. (C) Close-up of the solution concentration gradient generator with three inlets.

layer was then treated with oxygen plasma and covered with a 100 μm thick glass coverslip, forming the microfluidic device.

C. Tension sensor preparation

The tension sensor design. The tension sensor was constructed with double-stranded DNA (dsDNA) engineering. One strand DNA was conjugated with fluorophore and biotin; the other was tagged with quencher and RGDfK ligand. Details can be found in a previous publication.[24] The DNA sequence is listed below.

ITS with 12 pN threshold (with Cy3-BHQ2 pair): 5′-/RGD/GGG CGG CGA CCT CAG CAT/BHQ2/-3′. 5′-/Cy3/ATG CTG AGG TCG CCG CCC/Bio/-3′.

ITS with 54 pN threshold (with Cy5-BHQ2 pair): 5′-/RGD/GGG CGG CGA CCT CAG CAT/BHQ2/-3′. 5′-G/Cy5/T/Bios/ATGATGAGGTCGCCGCCC/-3′.

Immobilization of integrin tension sensors on channel surface. 200 μg ml^{-1} BSA-biotin was coated on the glass surface for 30 min and then 100 μg ml^{-1} neutravidin was flooded in the channel for 30 min, which was followed by incubation of biotin-tagged tension sensor at 0.1 μM concentration. Note that washing with PBS was performed between steps.

D. Washed platelet preparation

Canine blood was drawn from healthy staff- or student-owned volunteer dogs whose owners provided informed consent with approval from the Iowa State University's Institutional Animal Care and Use Committee and complied with ISU IACUC guidelines. The dogs were cared for as outlined in the NIH guide for the care and use of laboratory animals. In brief, 2 ml of blood was drawn from a dog's cephalic vein into a 3 mL syringe containing acid citrate dextrose (ACD) buffer (ACD buffer: 135 mM glucose, 75 mM sodium citrate, 38 mM citric acid) in a 1 : 9 ratio and then transferred to a 15 ml Falcon tube containing an equal volume of buffered saline glucose citrate (BSGC: 129 mM NaCl, 14 mM Na_3citrate, 11 mM glucose, 10 mM NaH_2PO_4, pH 7.3). ACD was the anticoagulant of choice to minimize Ca^{2+}-dependent platelet activation prior to washing the platelets free of plasma. Platelet-rich plasma (PRP) was generated by spinning this blood/BSGC mixture at room temperature at 170*g* for 8 minutes. The resulting supernatant was harvested as PRP. Platelets were isolated from PRP using centrifugation with washing buffer (113 mM NaCl, 4.3 mM K_2HPO_4, 4.2 mM Na_2HPO_4, 24.3 mM NaH_2PO_4, 5.5 mM dextrose, pH 6.3) to remove the unwanted components such as anti-coagulants, and fibrinogen and 100 units per ml apyrase (product # A6237, Millipore Sigma) and 1 mM PGE1 (product # P5515, Millipore Sigma) were added to prevent immediate activation during washing. Then, the fresh platelets were resuspended in F12 medium (HFL05, Caisson Laboratories) without phenol red. This resuspension restored Ca^{2+} to a concentration required for platelet function similar to ionized calcium available in citrated PRP.

Unless specifically mentioned otherwise, washed platelets were used for the following experiments. In addition to using washed platelets for most of our experiments, platelet force maps were also observed by plating just ACD anticoagulated whole blood samples with added ADP (platelet agonist) on the integrin tension sensor coated glass substrate.

E. Observation of platelet activity in flowing status

The recording of platelet activity was done using an epifluorescence microscope. The ADP addition and platelet flow were controlled by a syringe pump (Harvard Apparatus, Inc.). ADP is a standard platelet agonist. We used a few different agonists in our initial ITS studies and ADP worked the best. ADP was added from the beginning of flow, and the video recording was started either from the flow beginning or from the initiation of platelet adhesion. Since the platelets could not adhere at a high flow rate without the aid of von Willebrand factor (vWF), and in order to study the effect of shear stress on platelet adhesion mediated through GPIIb/IIIa (also called integrin $\alpha_{IIb}\beta_3$) alone, the shear rate was set at relatively low levels *i.e.* 1, 5, 10, and 100 s^{-1}.

F. ROCK inhibitor test with microfluidic-force mapping system

Previously, we tested the inhibition of platelet integrin molecular tensions, the forces transmitted by integrin molecules by tirofiban (GPIIb/IIIa inhibitor) at static status.[24] However, the force generation during the adhesion process of flowing platelets remained unknown. Here, the platelets with or without Y-27632 were pumped through micro-channels coated with integrin tension sensor.

G. Statistical analysis

The photos or videos were processed and analyzed using MATLAB (code is available upon request). All the data were presented as mean ± SD if applicable. The analysis of platelets was based on at least three independent

experiments and the sample size for platelet in each assay was more than 10.

Results and discussion

A. Effects of the flow rate on the platelets in microfluidic chips

The chip illustrated in Fig. 2 was used for the measurements summarized in this section. A photo of the corresponding fabricated chip is shown in Fig. 5A.

Modeling results of the flowing shear stress on platelets. A calculated representative velocity profile is shown in Fig. 4A. Clearly, the magnitude of the velocity in the narrow region is higher than that in the wide region. Using the point of an evaluation method in COMSOL and the relationship spf.mu (vx + uy), the average flowing shear stress magnitude around and on the platelets was calculated (Fig. 4B and C). The simulation results revealed that (i) the solution has a higher velocity in the narrow region (CH_n) than in the wide region (CH_W) of the microchannel and (ii) the shear stress on the platelets in the narrow region is higher than that in the wide region, indicating that the platelets in the narrow region can be more readily flushed away before the platelets were linked to the ITS (Fig. 1A) than those in the wide region. Based on the simulation results of the symmetrical structure (*i.e.* wide channel to narrow channel to wide channel) of the chip (Fig. 4B), the profile of flowing shear stress on the platelets is essentially similar for the solution flowing from the narrow region to the wide region in the microchannel and *vice versa*.

Recorded integrin molecular tension by time. First, the whole process of platelet adhesion and retraction at the single molecule level was monitored using a microfluidic chip (Fig. 5A). The uneven distribution of integrin tension in platelets and the lateral force signal was directly observed. This phenomenon was consistent with previous studies,[24,39] namely the polarity and the anisotropy of platelet adhesion force. As the platelets changed morphology during activation and formed extrusions of blebs and spikes, it was observed that the reshaped platelets tended to adhere and contract at the extrusion sites. Note that although the flow changed the platelet adhesion time, hence a longer time was required for

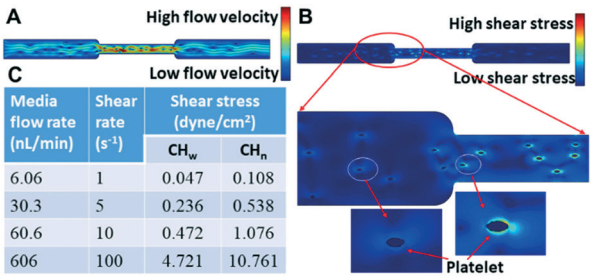

Media flow rate (nL/min)	Shear rate (s^{-1})	Shear stress (dyne/cm²)	
		CH_w	CH_n
6.06	1	0.047	0.108
30.3	5	0.236	0.538
60.6	10	0.472	1.076
606	100	4.721	10.761

Fig. 4 (A) Representative velocity profile inside the wide and narrow microchannels. (B) Representative flowing shear stress profile inside the wide and narrow microchannels. (C) The calculated flowing shear stress on the platelets at different solution flow rates into the chip and the different regions of the microchannels.

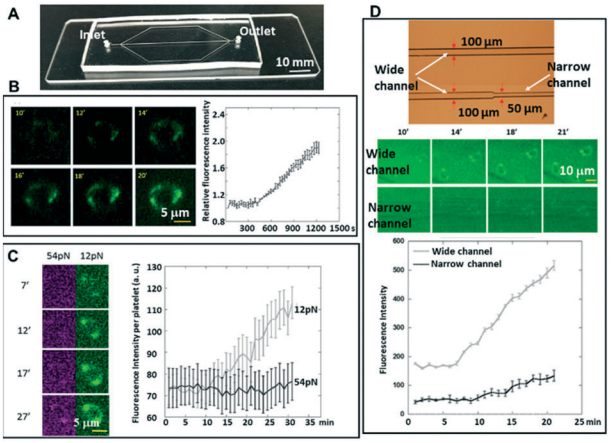

Fig. 5 (A) Photo of a microfluidic chip with straight microfluidic channels. (B) Integrin tension dynamics over time at 5 s^{-1}. The active platelets were flowed and adhered to the 12 pN integrin tension sensor surface. The increase of force signal was monitored (left). The fluorescence intensity per cell was quantified over time (right). (C) Two-level integrin tension dynamics over time at 5 s^{-1}. Activated platelets were flowed and adhered to the surface immobilized with both 12 pN ITS and 54 pN ITS. The increase of force signal was monitored. The fluorescence intensity at selected frames is shown (left) as well as the quantified fluorescence intensity per cell over time (right). The high integrin tensions occurred later compared to low integrin tension, which may reflect that platelets that adhere and spread do not require high integrin tension, but that the contraction process requires high integrin tension under shear stress. (D) The integrin tension for platelets at the stenotic region (narrow channel region) *vs.* the non-stenotic region. Shown are optical micrographs of the microfluidic channels on the chip (top), the force signal at selected frames (middle), and the quantified fluorescence intensity per cell over time (bottom).

platelet adhesion compared to the platelets under no-flow conditions in our previous study,[24] their integrin force pattern was not altered at a low flow rate. The force pattern is the ITS rupture pattern for individual platelets as clearly shown in Fig. 5B. It is measured by calculating the ITS rupture intensity for single platelets for a data set of 50 platelets. Analysis of ITS rupture intensity is done using MATLAB mentioned in our previous publication.[40]

Two-level integrin tensions for platelets under shear stress. For non-flowing platelets, two levels of integrin tensions in platelets have been observed,[24] which correspond to the platelet adhesion, spreading and retraction processes. As mentioned in ref. 24, the tension threshold for ITS (tunable in the range of 10–60 pN) activation was tuned to image integrin molecular tensions at different force levels. For low-level integrin tension, platelet force maps of integrin tensions above 12 pN were obtained as platelets could mechanically separate 18 bp DNA in an unzipping geometry. To monitor high-level integrin tensions, ITS with a 54 pN tension threshold was prepared since the platelets could rupture 18 bp dsDNA in a shear geometry. A typical ring-shaped force distribution clearly showing two or three force foci was observed for 12 pN ITS, while 54 pN ITS showed a dot pattern and more concentrated force map. For platelets,

it is much easier to rupture 12 pN ITS (weaker ITS) first than 54 pN ITS, and platelets will try to consume weaker ITS first before moving on to stronger ITS. Experimental results demonstrate that platelets employ low-level integrin molecular tensions (12–54 pN) for adhesion and high-level integrin molecular tensions (>54 pN) for contraction.

To test whether the flowing platelets still show two-level integrin tensions, platelets activated with ADP were flowed at 5 s^{-1} through the microchannels, which were coated with two types of tension sensors (12 pN and 54 pN sensors), simultaneously. It was found that even under shear stress, the platelets still finished the process of adhesion and spreading, which did not generate high integrin tension (>54 pN) at the initial adhesion stage, but high integrin tension occurred later in 2–10 minutes after initial adhesion (Fig. 5C).

Whole blood can also be used instead of isolated platelets in our flow model. In our previous experiments, we have observed that ITS rupture intensity remains at the same level if we utilized whole canine blood instead of using washed platelets (Fig. S1 in the ESI†). The only difference is that numerous red blood cells will be floating around if we plate whole blood instead of washed platelets, and the number of platelets per um^2 will be low. Also, red blood cells would not be able to adhere to the ITS-coated substrates unlike platelets (using binding of platelet integrins to RGD in ITS). Fig. S1† shows platelet force maps on the ITS-coated substrate (T_{tol} = 12 pN) using whole blood and washed platelets.

Stenosis mimicking chips for integrin tension study. It is well known that platelets tend to accumulate at the post-stenotic region in blood vessels,[41] as observed in *in vitro* experiments. In order to test whether integrin tension mapping could provide new details, the stenosis mimicking microfluidic channels (Fig. 5D) were utilized. During the flow process at 1 s^{-1}, the integrin signal was acquired. It was observed that platelets were able to adhere at the post-stenotic region (wide microchannel) by ~3 minutes sooner than at the stenotic region (narrow microchannel) (Fig. 5D), and the corresponding occlusion rate is 50%. Although the flow rate is not the same as that in the blood vessel, and the platelet adhesion *in vivo* is mediated by a series of events as well as different ligand–receptor interactions, this mimicking experiment qualitatively verified the adhesion preference for platelets in the post-stenosis region.

Effect of shear stress on integrin-mediated platelet adhesion and integrin activity. As shown in Fig. 5D, it was observed that the adhesion of the platelets was delayed at the stenotic region, *i.e.* the platelet adhesion was postponed due to higher shear stress by the narrower microchannel (mimicking the stenotic region), consistent with the simulation results in Fig. 4B and C. In order to verify whether the shear stress influences the platelet adhesion mediated by integrins, different shear stresses (*i.e.* flow rates) were applied during the experiments. In the first condition, the active platelets were flowed without pre-adhesion. The fluorescence intensity was measured and normalized to its baseline; the relative fluorescence intensity reflected the adhesion strength

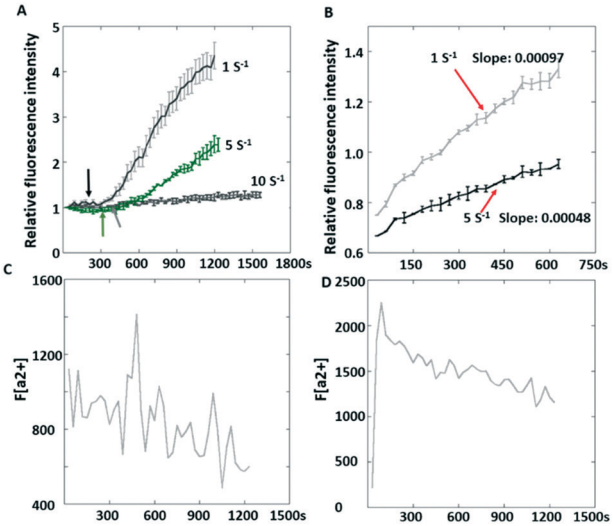

Fig. 6 The shear stress postponed the integrin-mediated platelet adhesion. The postponed integrin signal could be explained by calcium oscillation. (A) The record of platelet adhesion from the beginning of flow; (B) the record of platelet adhesion after initial adhesion followed by shear flow; (C) Ca^{2+} fluctuation at 1 s^{-1}; (D) Ca^{2+} transient at 5 s^{-1}.

of platelet adhesion. As shown in Fig. 6A, the flowing platelets at 1 s^{-1} resulted in the earliest fluorescence signals in comparison with those at 5 s^{-1} and 10 s^{-1}, and the flowing platelets at 5 s^{-1} resulted in fluorescence signals earlier than those at 10 s^{-1}. Because platelet adhesion is mediated by integrins which form bonds with the RGD ligands on the tension sensors, the on-rate of the integrin–ligand bond determines the initial force overcoming the effect of shear stress. Hence, a larger shear force generated by a higher flow rate would reduce the platelet adhesion rate.

It was also observed that the increasing rate of the fluorescence intensity (indicating how actively the integrin tensions are generated in platelets) was different after platelet adhesion at different flow rates. To avoid inaccurate comparison due to sampling, the platelets were allowed to adhere first prior to shear flow. Interestingly, the slopes of fluorescence increment over time were still different, with a larger slope (0.00097) at 1 s^{-1} compared to 0.00048 at 5 s^{-1} (Fig. 6B). This phenomenon may be attributed to the normal stress acting on platelets inhibiting actomyosin assembly due to the ventral integrins' decreased outside-in signaling. We observed that Ca^{2+} fluctuation was found at 1 s^{-1} but not at 10 s^{-1} (Fig. 6C), which indicates that the integrin $\alpha_{IIb}\beta_3$ was not activated since Ca^{2+} oscillation occurs with firm platelet adhesion.[30] The Ca^{2+} transient (Fig. 6D) suggested a low level of integrin $\alpha_{IIb}\beta_3$ activation.

Platelet activity under shear stress in platelet aggregates. It is known that the interplay between platelets favors platelet stable adhesion and aggregation.[42] In order to test the interaction between platelets, we studied the adhesive force of aggregating platelets at 100 s^{-1} shear rate. It was observed that platelets hardly adhered to an RGD-coated surface at 100 s^{-1} (data not shown). However, if platelet aggregates were

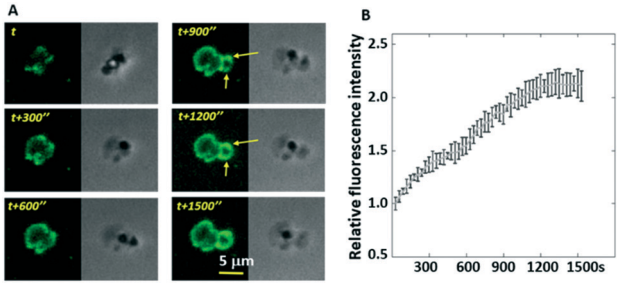

Fig. 7 The recording of the single platelet activity at a platelet aggregate in a flowing channel. (A) A platelet disengaged itself from the clump, spread on the substrate and generated integrin tensions. The rolling platelet still produces integrin tensions in a circular pattern with appreciable force polarity (marked by yellow arrows). (B) The increase of fluorescence intensity (indicating integrin activity in platelets) of a platelet aggregate under a shear rate of 100 s^{-1}.

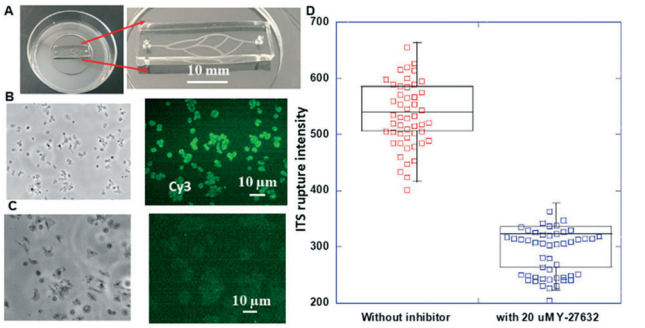

Fig. 8 (A) Picture of one blood-vessel-mimicking chip and its close-up photo; (B) optical micrograph and fluorescence image of the integrin tension sensors without inhibitor (Y-27632) treatment; (C) optical micrograph and fluorescence image of the integrin tension sensors with 20 μM inhibitor (Y-27632) treatment. (D) The measured fluorescence intensity with and without inhibitor (Y-27632) treatment.

allowed to form prior to applying shear stress, the involved platelets showed the ability to bear against the shear stress and finally adhere and transmit the integrin tension as shown in Fig. 7. It was found that some platelet–platelet interactions could not overcome the shear stress and disconnected from each other, and tightly linked platelets may disengage themselves from the aggregate and commence the adhesion, spreading, and contraction processes. The rolling platelets still showed force polarity, following lateral-circular patterns as demonstrated by the arrows. The interaction between platelets either sends some biochemical signals to the first-adherent platelets or co-activates through the mechanical force. The platelets de-granulate[43,44] and release platelet activating factors such as ADP and thromboxane during the aggregation process.[45–49] The activated platelet binds to neighboring platelets through GPIIb/IIIa–fibrinogen–GPIIb/IIIa complexes, and the tension on GPIIb/IIIa may further reciprocate the retraction by triggering the actinomyosin (re)assembly[49] and accelerating the aggregation process.[50]

It has been well known that during systole inside the coronary arteries, the blood flow is pulsatile with zero or reversing flow,[51] indicating that the shear stress is pulsatile and thus changes over time. Given that the shear stress also depends on the locations, sizes and shapes of the blood vessels, in order to analyze the behaviors of platelets more accurately, it is important to study their spatiotemporal behaviors inside the blood vessel mimicking chip. To this end, for future work, a similar piezoelectric pumping system as reported in ref. 52 can be adopted for monitoring the pulsatile flow effect on the platelets.

B. Y-27632 (ROCK inhibitor) treatment on platelets in a blood vessel mimicking chip

The chips illustrated in Fig. 3 were used for the measurements summarized in this section. The photos of the corresponding fabricated chips are shown in Fig. 8A and 9A.

Y-27632 treatment in a blood vessel mimicking chip. In this assay, 12 pN integrin tension sensors were grafted on the inner surfaces of the microchannels on the microfluidic chip.[24] A uniform ITS concentration of 0.1 μM has been consistently used throughout the experiments and all other conditions such as incubation time were kept the same. Also, the microfluidic device was first coated with 0.1 μM biotin-ssDNA-Cy3 as a control experiment to visualize the fluorescence signal. The optical and fluorescence images are shown in Fig. S2 in the ESI.† As mentioned in our previous work,[24] control experiments were performed to make sure that integrins activate the ITS, and RGD is essential for ITS activation. After that, the chip was washed and filled with 1× PBS. Washed platelets were used for this experiment and the platelet solution was injected at a flow rate of 5–10 μl min^{-1} and incubated for 15 min. Finally, inhibitor (Y-27632) spiked serum and phenol red free Ham's F-12 medium was injected into the chip. We have used phenol red free medium throughout the experiment to avoid background fluorescence

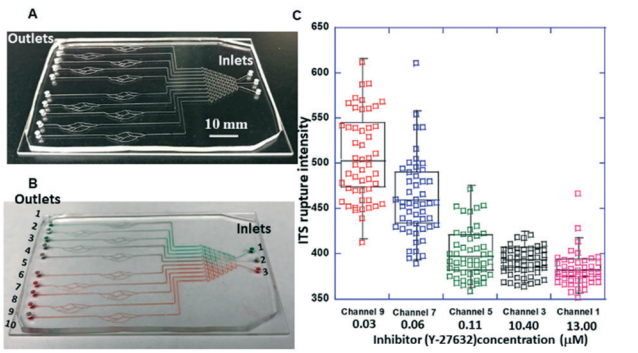

Fig. 9 (A) Photo of one microchip with 10 blood-vessel-mimicking channels with a solution concentration gradient generator; (B) optical micrograph showing different concentrations of the inhibitor (food dyes were used for visibility) flowed into 10 blood vessel mimicking channels (channel # 1–10); (C) the measured fluorescence intensity with inhibitor (Y-27632) treatment of different concentrations automatically generated by the solution concentration gradient generator on chip.

caused by phenol red. The fluorescence images were taken after 40 min of incubation.

A picture of the fabricated chip is shown in Fig. 8A. A representative optical micrograph and its corresponding fluorescence image of the integrin tension sensors in the microfluidic channel are shown in Fig. 8B, and a representative optical micrograph and corresponding fluorescence image of integrin tension sensors after the treatment with Y-27632 at a concentration of 20 μM are shown in Fig. 8C. As shown in Fig. 8D, after the Y-27632 treatment, the fluorescence intensity dropped significantly, indicating that the tension force induced by the platelets on the dsDNA integrin tension sensors was reduced. These results confirmed that Y-27632 can effectively reduce integrin tensions in adherent platelets.

Y-27632 treatment at a series of concentrations. In order to evaluate the effect of Y-27632 treatment at a series of concentrations simultaneously, ten blood vessel chips with an integrated solution concentration gradient generator have been used. The photo of the chip is shown in Fig. 9A. As a demonstration of the concentration gradient generator, an inhibitor model (blue food dye and red food dye) is flowed into inlet 1 and inlet 3, and water is flowed into inlet 2. As shown in Fig. 9B, a series of concentrations (*i.e.* 10 different concentrations) of the inhibitor model (food dyes) are generated in ten blood vessel chips. In the Y-27632 treatment experiments, 20 μM Y-27632 is applied to inlet 1; water is applied to both inlet 2 and inlet 3. As a result, Y27632 at ten different concentrations was flowed into ten blood vessel chips.

To accurately determine the concentrations generated by the concentration gradient generator, high-performance liquid chromatography (HPLC) was used to determine the concentrations of the Y-27632 flowed into the blood vessel chip. To this end, the Y-27632 solutions were first collected from the outlets of the gradient generator, and then their concentrations were measured, respectively. The measured fluorescence intensities of the integrin tension sensors after the treatment of different concentrations of Y-27632 are given in Fig. 9C. The coefficient of variation (CV) in Fig. 9C is always less than 1. For example, for a Y-27632 concentration of 0.03 μM, the CV is ~0.1. Y-27632, the selective ROCK inhibitor, has an IC50 value of 600 nM as provided by the manufacturer (Tocris Bioscience, Inc.).

Clearly, the higher the Y-27632 concentration was, the lower the fluorescence intensity of the integrin tension sensors the platelets produced. Washed platelets were used for this experiment. This result indicates that Y-27632 can reduce integrin tensions in platelets during adhesion and may also effectively decrease platelet aggregation and inhibit thrombus formation as these two processes are also mediated by integrins.[53,54] Since this chip can be readily scaled up for high-throughput applications, these results indicate that this type of chip can be potentially used (i) for determining the optimal concentration and/or dose of a ROCK inhibitor and/or an antiplatelet drug for optimal treatment and (ii) for screening possible drug candidates for platelet-related diseases.

Conclusions

Microfluidic chips have been developed for the first time to study the behaviors of platelets by combining microfluidics and molecular tension sensors. Using these chips grafted with the integrin tension sensors on the inner surfaces of microchannels, integrin $\alpha_{IIb}\beta_3$ force maps in platelets under low flow status ($<1000\ s^{-1}$) have been obtained. Specifically, these chips allow us to mimic blood vessel occlusion and to study the integrin tension affected by flow rate, namely, the effect of the shear stress on platelets, which can decrease the adhesion activity due to the decreased integrin $\alpha_{IIb}\beta_3$ activation reflected by measurements of calcium oscillations and with the tension sensor. The effect of ROCK inhibitor Y27632 on platelets has also been studied with these chips, suggesting their potential in platelet assays for high-throughput applications. Hence, using these chips, it is possible to screen drug candidates for medications that either inhibit or promote platelet function and thus optimize drug concentrations for the treatment of platelet-related diseases.

Author contributions

S. Mao, A. Sarkar: chip fabrication and experiments, data analysis, review and editing. Y. Wang, C. Song: experiments, data analysis. D. LeVine: platelet sample preparation, review and editing. X. Wang: conceptualization, writing – original draft, review and editing. L. Que: conceptualization, writing – original draft, review and editing.

Conflicts of interest

There are no conflicts to declare.

Acknowledgements

The authors acknowledge the funds from the McGee-Wagner Interdisciplinary Research Award at Iowa State University and the National Institutes of Health (1R35GM128747). The authors thank the technical staff at Iowa State University for the measurement of the concentrations of ROCK inhibitor Y-27632 using high-performance liquid chromatography (HPLC). The authors would like to thank the volunteer dogs for sharing their platelets and the technicians of the Small Animal Internal Medicine Service at Iowa State University for helping to obtain blood samples.

References

1 R. Tracy, *Chest*, 2003, **124**(3), 49S.
2 G. Raskob, *et al.*, *Arterioscler., Thromb., Vasc. Biol.*, 2014, **34**(11), 2363.
3 G. Davì and C. Patrono, *N. Engl. J. Med.*, 2007, **357**(24), 2482.

4 S. Willoughby, A. Holmes and J. Loscalzo, *Eur. J. Cardiovasc. Nurs.*, 2002, **1**(4), 273.
5 M. Packham, *Can. J. Physiol. Pharmacol.*, 1994, **72**(3), 278.
6 K. Ouriel, *et al.*, *J. Vasc. Surg.*, 1991, **14**(6), 757.
7 C. Chen, *J. Cell Sci.*, 2008, **121**(20), 3285.
8 W. Lam, *Nat. Mater.*, 2011, **10**(1), 61.
9 D. Myers, *et al.*, *Nat. Mater.*, 2007, **16**(2), 230.
10 W. Wang and M. King, *Ann. Biomed. Eng.*, 2012, **40**(11), 2345.
11 M. H. Kroll, *et al.*, *Platelets and shear stress*, 1996.
12 Z. Ruggeri, *et al.*, *Blood*, 2006, **108**(6), 1903.
13 J. Bennett, B. Berger and P. Billings, *J. Thromb. Haemostasis*, 2009, **7**, 200.
14 M. Moser, *et al.*, *Nat. Med.*, 2008, **14**(3), 325.
15 J. Rivera, *et al.*, *Haematologica*, 2009, **94**(5), 700.
16 J. Gibbins, *J. Cell Sci.*, 2004, **117**(16), 3415.
17 Z. Li, *et al.*, *Arterioscler., Thromb., Vasc. Biol.*, 2010, **30**(12), 2341.
18 M. Moroi and S. M. Jung, *Front. Biosci., Landmark Ed.*, 1998, **3**, 719–728.
19 S. Jackson, W. Nesbitt and E. Westein, *J. Thromb. Haemostasis*, 2009, **7**, 17.
20 V. Karagkiozaki, *et al.*, *Nanomed.: Nanotechnol., Biol. Med.*, 2009, **5**(1), 64.
21 M. Hussain, A. Agnihotri and C. Siedlecki, *Langmuir*, 2005, **21**(15), 6979.
22 D. Myers, *et al.*, *Nat. Mater.*, 2017, **16**(2), 230.
23 S. Henriques, *et al.*, *J. Cell Sci.*, 2012, **125**(16), 3914.
24 Y. Wang, *et al.*, *Biosens. Bioelectron.*, 2018, **100**, 192.
25 X. Wang and T. Ha, *Science*, 2013, **340**(6135), 991.
26 Y. Wang and X. Wang, *Sci. Rep.*, 2016, **6**(1), 1.
27 A. Sarkar, *et al.*, *Curr. Biol.*, 2020, **30**(20), 4022.
28 Y. Zhang, *et al.*, *Nat. Commun.*, 2014, **5**(1), 1.
29 Y. Liu, *et al.*, *Proc. Natl. Acad. Sci. U. S. A.*, 2016, **113**(20), 5610.
30 J. Sánchez-Cortés and M. Mrksich, *Chem. Biol.*, 2009, **16**(9), 990.
31 P. Litjens, *et al.*, *J. Thromb. Haemostasis*, 2005, **3**(6), 1274.
32 D. LeVine, *et al.*, *Br. J. Haematol.*, 2014, **167**(1), 110.
33 K. Son, *Clin. Hemorheol. Microcirc.*, 2010, **44**(1), 27.
34 M. Boudreaux, *Transl. Res.*, 2007, **150**(2), 81.
35 A. Hill, *et al.*, in *Handbook of cardiac anatomy, physiology, and devices*, Springer, Cham, 2015, pp. 89–114.
36 P. Camacho, *et al.*, *J. Cardiovasc. Dev. Dis.*, 2016, **3**(4), 30.
37 M. Wilkerson, *et al.*, *Vet. Clin. Pathol.*, 2001, **30**(3), 141.
38 X. Li, H. Yin and L. Que, *Biomed. Microdevices*, 2014, **16**(5), 771.
39 Y. Zhang, *et al.*, *Proc. Natl. Acad. Sci. U. S. A.*, 2018, **115**(2), 325.
40 A. Sarkar, D. LeVine, Y. Zhao, K. Mollaeian, J. Ren and X. Wang, *bioRxiv*, 2020, DOI: 10.1101/2020.01.24.918946.
41 E. Westein, *et al.*, *Proc. Natl. Acad. Sci. U. S. A.*, 2013, **110**(4), 1357.
42 W. Nesbitt, *et al.*, *J. Cell Biol.*, 2003, **160**(7), 1151.
43 P. Blair and R. Flaumenhaft, *Blood Rev.*, 2009, **23**(4), 177.
44 E. Golebiewska and A. Poole, *Blood Rev.*, 2015, **29**(3), 153.
45 T. Abshire and S. Jobe, Overview of the Coagulation System, in *Transfusion Medicine and Hemostasis*, Elsevier, 2009, pp. 431–438.
46 S. Yun, *et al.*, BioMed research international, 2016, vol. 2016.
47 D. Woulfe, J. Yang and L. Brass, *J. Clin. Invest.*, 2001, **107**(12), 1503.
48 A. Chu, *Int. J. Inflammation*, 2011, **2011**, 367284.
49 M. Murrell, *et al.*, *Nat. Rev. Mol. Cell Biol.*, 2015, **16**(8), 486.
50 F. Albert and F. N. Christopher, *JRSM Cardiovasc. Dis.*, 2012, **1**(2), 1.
51 Y. Huo and G. Kassab, *Am. J. Physiol.*, 2006, **291**, H1074–H1087.
52 M. Mohammed, *et al.*, *Anal. Chem.*, 2019, **91**, 12077.
53 J. Sweeny, D. Gorog and V. Fuster, *Nat. Rev. Cardiol.*, 2009, **6**(4), 273.
54 P. Harrison, *et al.*, *Thromb. Res.*, 2007, **120**(3), 323.